

# CHARACTERISTICS OF THE INTRASEASONAL VARIABILITY OF PRECIPITATION OVER EASTERN ARGENTINA

Paula L. M. González \* , Carolina S. Vera  
CIMA, UBA-CONICET, Buenos Aires, ARGENTINA.

Brant Liebmann  
NOAA-CIRES Climate Diagnostics Center, Boulder, USA.

## ABSTRACT

An analysis of the intraseasonal variability of precipitation over central and eastern Argentina is presented. Daily precipitation data from Argentinean Weather Service stations that are representative of the different geographical regions have been used for the period 1976-2001. The climatological mean seasonal cycle was first removed from the timeseries. In order to retain the intraseasonal variability associated with the warm season (1 Nov-31 Mar), the anomaly timeseries were normalized and filtered by a 20-90 day Lanczos filter. Daily OLR data for the period 1979-2001 were also used to compare its associated intraseasonal variability with that depicted by the precipitation data.

Results show that intraseasonal variability of the daily precipitation observed over central and eastern Argentina explains a significant portion of the total summer variance. Moreover, the explained variance by the intraseasonal variability is largest over eastern Argentina, from subtropical to middle latitudes. OLR, typically used as summer precipitation proxy, is able to reproduce the basic characteristic of the precipitation intraseasonal variability particularly when the amplitude of the intraseasonal oscillations (IO) in precipitation timeseries is relatively large. Although, when the IO amplitude is small, OLR variability only explains a small fraction of the precipitation variability. Furthermore, the OLR is not able either to represent the precipitation variability on synoptic timescales.

Positive (negative) events of precipitation intraseasonal variability were defined identifying the dates in which the filtered precipitation series exhibit values above (below) one standard deviation for at least 5 days. Around 50 events were identified for each category over the period considered, with around half of them exhibiting a mean length of 7 days and the others of 12 days. The date associated with the maximum (minimum) filtered precipitation value was identified for each positive (negative) event that was then considered as Day 0 in the computation of daily composites.

Composites 200-hPa geopotential-height anomalies for positive precipitation events occurred over subtropical eastern Argentina show a wave train evolving all along the South Pacific over the 10-day period previous to the precipitation peak. The wave train is characterized by quasistationary anomaly centers and a relatively fast eastward wave energy progression. On the other hand, composites for positive precipitation events over extratropical eastern Argentina are associated with the evolution of long-life synoptic waves progressing eastward.

Composites of OLR anomalies for positive precipitation events over both subtropical and extratropical eastern Argentina are associated with decreased convection in the SACZ region, in agreement with previous works. Nevertheless, differences in the location and timing of the OLR positive anomalies over the SACZ region were observed for both types of composites that will be further discussed in the Conference.

---

## 1. INTRODUCTION

Over tropical and subtropical South America most of the annual precipitation occurs during the warm season, in groups of heavy rain showers and thunderstorms that are associated to synoptic and mesoscale time scales. During that season, the analysis of the outgoing longwave radiation (OLR) anomalies over those areas reveals a dipole pattern, known as the South American Seesaw (SASS) with variability on intraseasonal time scales.

The SASS pattern shows a center of activity over southeastern Brazil, near the climatological position of the South Atlantic Convergence Zone (SACZ), and another center over the northeast of Argentina, south of Brazil, Uruguay and Paraguay (Nogues-Paegle y Mo, 1997). Events of active (inactive) SACZ appear to be related to an intense (weakened) southward moisture flux, and consequently to inhibited (enhanced) precipitation in subtropical regions.

Nogues-Paegle et al. (2000) found that the SASS pattern exhibits intraseasonal variability that is mainly restricted to two distinct bands,

---

\* *Corresponding author address:*  
Paula L. M. González, CIMA, CONICET-UBA,  
E-mail: [pgonzalez@cima.fcen.uba.ar](mailto:pgonzalez@cima.fcen.uba.ar) .

† *Corresponding author address:*

---

Paula L. M. González, CIMA, UBA - CONICET,

with periods ranging between 20-28 days, and between 36-40 days.

Recently, Liebmann et al. (2004) found that the Madden-Julian Oscillation (MJO), a global oscillation with variability in the 30-to-60-days band, explains a part of the fluctuations of the SASS pattern. Positive precipitation anomalies in southeastern South America (in the SACZ) tend to occur nearly 2 days (26 days) after the MJO peaks in the tropical western Pacific. This result is particularly relevant since the MJO is the only intraseasonal oscillation with demonstrated levels of predictability (e.g.: Ferranti (1990)), and then constitutes a strong motivation for studying intraseasonal variability of precipitation in Argentina.

Most studies on the subject of intraseasonal variability in southeastern South America have been based on OLR anomalies, usually used as a proxy for tropical convection. Nevertheless, OLR anomalies may not be an adequate tool when monitoring precipitation in subtropical regions. Liebmann et al. (2004) found, using observed precipitation data that OLR anomalies have deficiencies in representing the influence of the MJO over precipitation in subtropical South America.

The lack of complete and extended daily precipitation datasets for the region, and the fact that precipitation is highly sporadic in the subtropics, has limited the attempts of studying intraseasonal variability through the use of filtered daily precipitation data.

The purpose of this work is to provide a first glance of the intraseasonal variability on daily precipitation series from Argentinean Weather Service stations.

## 2. DATA AND METHODOLOGY

### 2.1 Data

For this study, daily precipitation timeseries from five Argentinean National Weather Service stations were selected for the period 1976 to 2001. The location of the stations is shown in Fig. 1 and their features presented in Table 1.

OLR timeseries were extracted from the nearest grid point to each station, using the interpolated OLR daily mean dataset, available from NOAA/CIRES/Climate Diagnostic Center (Liebmann and Smith, 1996). Due to satellite failure, the chosen timeseries belong to the period 1979 to 2001.

When exploring the dynamics of intraseasonal variability, 200-hPa and 850-hPa geopotential height fields from the NCEP-NCAR reanalysis datasets (Kalnay et al., 1996) were also used.

As it has been previously shown by several authors (Nogues-Paegle and Mo 1997;

Liebmann et al. 1999; Nogues-Paegle et al. 2000), intraseasonal variability over South America is particularly active during summer. Thus, the period 1 November to 31 March was selected as representative of the warm season in the region under study. The period was chosen to be longer than the chronological summer to accomplish a better description of intraseasonal events.



FIG. 1. Location of the selected Weather stations (red dots).

TABLE 1. Features of analysed weather stations.

LONGITUDE	LATITUDE	NAME	PROVINCE	ALTITUDE (m)
-65.02	-26.8	TUCUMÁN OBSERVATORIO	TUCUMÁN	480
-58.46	-27.27	CORRIENTES AERO	CORRIENTES	62
-57.6	-30.26	MONTE CASEROS AERO	CORRIENTES	54
-60.48	-31.78	PARANÁ AERO	ENTRE RÍOS	78
-58.5	-34.8	EZEIZA AERO	BS AIRES	20

### 2.2 Pre-processing of precipitation data

Since precipitation in the subtropics is usually highly non-Gaussian, seasonal anomalies were transformed to standardized Gaussian deviates using a probability-integral transformation, described in Sardeshmukh et al. (2000). This procedure should always be considered when attempting to use certain statistic tools such as correlations which require timeseries to be Gaussian.

### 2.3 Filtering

Intraseasonal variability was isolated using a band-pass Lanczos filter (Duchon 1979), with 101 weights. When needed, Lanczos high-pass and low-pass filters with the same number of weights were also used.

Both precipitation transformed seasonal anomalies and OLR seasonal anomalies were filtered to retain 20-to-90-day variability.

## 3. RESULTS

### 3.1 Variance analysis

A variance analysis was performed to precipitation and OLR timeseries for each station. The results, as presented in Table 2,

show that the seasonal cycle explains the lowest percentage of precipitation variability (Table 2a). This is coherent with the fact that a single season was considered. It can be noted, however, that clear differences exist between Tucumán, with a distinct summer rainy season, and those stations located further east, with a transition regime between summer and winter precipitation (e.g. González and Barros 1996).

The percentages of variance explained by the seasonal cycle for OLR are also the lowest (Table 2b). The values for Ezeiza are, however, particularly high. This feature is probably explained by the fact that this station is located further south and OLR anomalies are not only related to convective activity, but can also be linked to upper level long-wave radiation emissions from cirrus and other non-precipitating clouds.

Transient variability explains, as expected, the highest percentages of variance, and it is mostly related to synoptic activity (periods of less than 20 days). It can be seen that the short-scale variability explains a higher percentage of precipitation variance (86% to 89.5%) than that of OLR variance (76.5% to 83%). The percentages of explained variance by intraseasonal and interannual variability are, however, greater in the case of OLR. Intraseasonal variability, in particular, explains 8.5% to 11% of OLR variance and 5.5% to 8.5% of precipitation variance.

Another particular result shows that Tucuman is the station that exhibits the lowest explained variance by intraseasonal variability. This is probably due to the fact that this station, located further west, is not under the influence of the SASS pattern activity. Besides, as it can be seen in Fig. 1, the station is located in a region of complex topography that provides distinctive

features to the precipitation events in the vicinity of the station.

The rest of the work will focus on the results for Monte Caseros station, since it is located in a region where the signal of the SASS pattern is assumed to be strong.

### 3.2 Relationship between precipitation and OLR

The relationship between precipitation and OLR was analyzed in detail for each station using correlations. The intention was to determine whether the OLR anomalies constitute an appropriate proxy for precipitation or not.

Correlations were computed for daily anomalies and for filtered daily anomalies of precipitation and OLR, over each summer season in the period 1979 to 2001.

The correlation significance was assessed through a t-test. Following Eshel et al, (2000) the t statistic was calculated as:

$$t = \sqrt{(df - 2)/1 - r^2}$$

where  $r$  is the correlation coefficient,  $df=N/t_i$  represents the series' degrees of freedom,  $N$  is the length of the series and  $t_i$  the independence time, estimated through the autocorrelation functions.

For the correlations between filtered anomalies, however, the degrees of freedom were more carefully assessed due to the oscillatory behavior that the filtering process prints on the series. In those cases, it was used:

$$df = \frac{N}{1 + 2(\bar{C}_{pp} \cdot \bar{C}_{OLR})}$$

where  $C_{pp}$  and  $C_{OLR}$  represent the autocorrelation vectors.

TABLE 2. Variance analysis for the period 1 November to 31 March.

a) Precipitation					
VARIANCE [mm <sup>2</sup> ]	Tucumán	Paraná	Corrientes	Mte. Caseros	Ezeiza
<b>total</b>	<b>213.923</b>	<b>172.620</b>	<b>221.752</b>	<b>201.996</b>	<b>98.326</b>
seasonal cycle	1.940 ( 0.91 % )	0.014 ( 0.01 % )	0.129 ( 0.06 % )	0.365 ( 0.18 % )	0.024 ( 0.02 % )
transients	211.504 ( 98.87 % )	172.541 ( 99.95 % )	221.648 ( 99.95 % )	201.686 ( 99.85 % )	98.271 ( 99.95 % )
less than 20 days	191.617 ( 89.57 % )	150.454 ( 87.16 % )	192.220 ( 86.68 % )	173.602 ( 85.94 % )	84.544 ( 85.94 % )
from 20 to 90 days	11.657 ( 5.45 % )	14.440 ( 8.37 % )	16.816 ( 7.58 % )	17.178 ( 8.50 % )	7.706 ( 7.84 % )
more than 90 days	3.177 ( 1.49 % )	3.475 ( 2.01 % )	4.816 ( 2.17 % )	4.407 ( 2.18 % )	2.202 ( 2.24 % )
b) OLR					
VARIANCE [(W/m <sup>2</sup> ) <sup>2</sup> ]	Tucumán	Paraná	Corrientes	Mte. Caseros	Ezeiza
<b>total</b>	<b>651.811</b>	<b>1026.761</b>	<b>1304.256</b>	<b>1355.755</b>	<b>1016.947</b>
seasonal cycle	11.078 ( 1.7 % )	8.537 ( 0.83 % )	2.077 ( 0.16 % )	7.297 ( 0.54 % )	21.086 ( 2.07 % )
transients	638.8 ( 98 % )	1022.112 ( 99.55 % )	1303.906 ( 99.97 % )	1352.201 ( 99.74 % )	996.207 ( 97.96 % )
less than 20 days	488.064 ( 74.9 % )	836.932 ( 81.51 % )	1029.794 ( 78.96 % )	1092.251 ( 80.56 % )	829.494 ( 81.57 % )
from 20 to 90 days	79.173 ( 12.15 % )	94.516 ( 9.21 % )	161.233 ( 12.36 % )	136.449 ( 10.06 % )	91.775 ( 9.02 % )
more than 90 days	38.816 ( 5.96 % )	45.353 ( 4.42 % )	37.76 ( 2.9 % )	58.896 ( 4.34 % )	32.306 ( 3.18 % )

Distinctive correlation values for Monte Caseros are shown in Table 3, along with some other parameters used for comparison. Bold values are significant at the 95 % level. The maximum value for each category is shown in red and the minimum in blue.

**TABLE 3.** Correlations between precipitation and OLR for Monte Caseros station.

SUMMER	ANOMALIES	FILTERED ANOMALIES	# DAYS WITH RAIN	ACCUMULATED PRECIPITATION (mm)
1983/1984	-0.31	-0.44	58	778.0
1997/1998	<b>-0.53</b>	<b>-0.88</b>	<b>59</b>	<b>1429.3</b>
2000/2001	-0.14	-0.63	46	767.6
<b>MEAN</b>	<b>-0.41</b>	<b>-0.66</b>	42	736.9

The minimum correlation between anomalies was registered in the 2000-2001 summer season (-0.14). The value is not significant and implies that less than the 2% of the daily variability of precipitation could be explained by the associated variability in OLR. The maximum value (-0.51) belongs to the 1997-1998 summer season and shows that 26% of daily variability in precipitation can be explained by OLR. There is no clear relationship between these values and the number of days with rain or the accumulated precipitation.

For filtered anomalies, the minimum correlation value was found in 1983-1984 summer season. Though significant, this value means that only a small part of the intraseasonal variability in the precipitation for this summer was related to that variability in OLR. The maximum value also belongs to the 1997-1998 season (-0.88) and implies an explained co-variability of more than 75%.

### 3.3 Case studies

To better understand the influence of intraseasonal activity over precipitation in the region under study, some particular summer seasons were analyzed in detail. The ones chosen for that purpose were 1983-1984 and 1997-1998 for showing the lowest and highest correlation between intraseasonal variability in precipitation and in OLR, respectively.

Figure 2a shows the evolution of the series during the season 1983-1984. The series belonging to standardized filtered OLR anomalies have inverted sign to simplify the comparison. That summer qualifies as a neutral ENSO event, according to Trenberth (1997), and it shows an accumulated precipitation value slightly higher than the average, with an elevated number of days with rain.

Wavelet analysis for this summer is presented in Figures 2b (precipitation) and 2c (OLR). It shows an intense activity of intraseasonal oscillations, with periods ranging from 30 to 40 days. The activity is present in both variables, but it starts earlier in the case of OLR. Besides, precipitation activity on intraseasonal scales is

restricted to the second half of the summer and also spans to shorter periods. The low correlation between the series appear to be explained by two facts: precipitation tends to have shorter scale variability and some sort phase shift exists between the two series.

The evolution of the series during 1997-1998 summer is shown in Figure 3a, and they clearly shows a better agreement than in the previous case. That season was one of the strongest ENSO events registered up to this moment, with particularly intense activity of the MJO in the tropical Pacific. It also registered the largest accumulated precipitation and the largest number of rainy days among all summers.

The series clearly show the modulating effect of the intraseasonal oscillations (IO) on precipitation events, and the agreement between the filtered series improves when those IO exhibit large amplitudes. Wavelet analysis (Figs. 3b and 3c) shows a greater agreement between precipitation and OLR intraseasonal activity, with periods of 30 to 40 days. In this case, the large correlation observed between the two series appears to be related to an intense activity of intraseasonal oscillations.

Similar analyses performed for the other stations (not shown) show also largest correlations during summers with intraseasonal oscillations of considerable amplitude.

### 3.4 Intraseasonal events

Events of intraseasonal variability were defined for precipitation and for OLR. Following Nogues-Paegle and Mo (1997), a *positive event* was defined when the standardized filtered variable became larger than the unity for at least five days. Similarly, a negative event was defined when the standardized filtered anomaly became smaller than minus the unity for a period of at least five days. A subdivision between *short* and *long* events was also made. The short events correspond to durations shorter than 10 days, while the long ones last for at least 10 days.

**TABLE 4.** Statistics of intraseasonal events in Monte Caseros station.

MONTE CASEROS		precipitation		OLR	
		#	mean length (days)	#	mean length (days)
positive	<b>TOTAL</b>	<b>48</b>	<b>9.7</b>	<b>59</b>	<b>8.6</b>
	short	25	7.3	39	7.3
	long	23	12.3	20	11.2
negative	<b>TOTAL</b>	<b>50</b>	<b>10</b>	<b>53</b>	<b>9.3</b>
	short	24	6.8	29	7.1
	long	26	13.3	24	11.9

The statistics for those events in Monte Caseros are shown in Table 4. It can be seen that there is an equivalent number of short and long events in precipitation. The same was

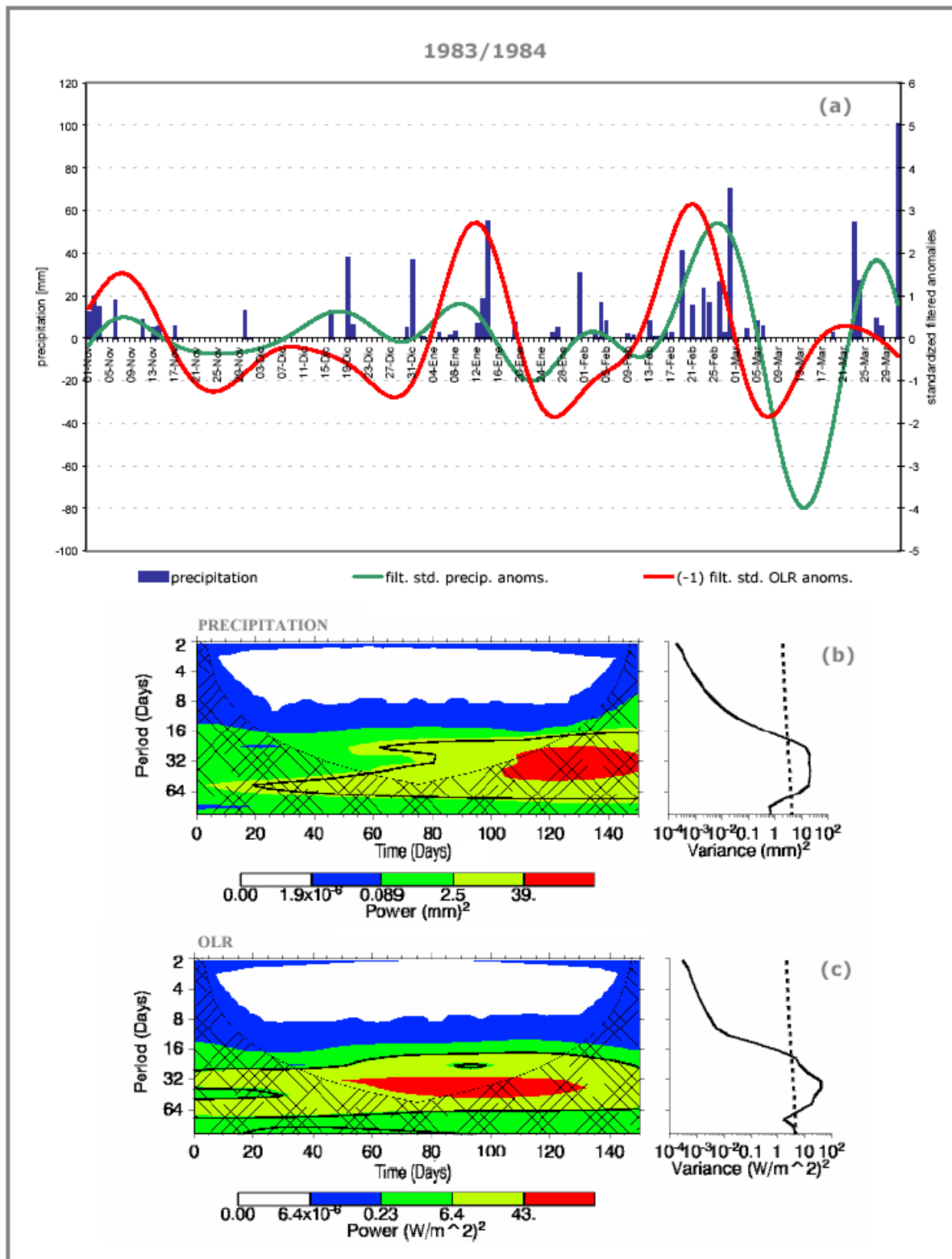


**Figure 2.** (a) Evolution of the timeseries during 1983-1984 summer season in Monte Caseros; (b) wavelet power spectrum and global wavelet for filtered precipitation; (c) wavelet power spectrum and global wavelet for filtered OLR. Black contour is the 5% significance level, using a white-noise background spectrum. The dashed line is the significance for the global wavelet spectrum, assuming the same significance level.

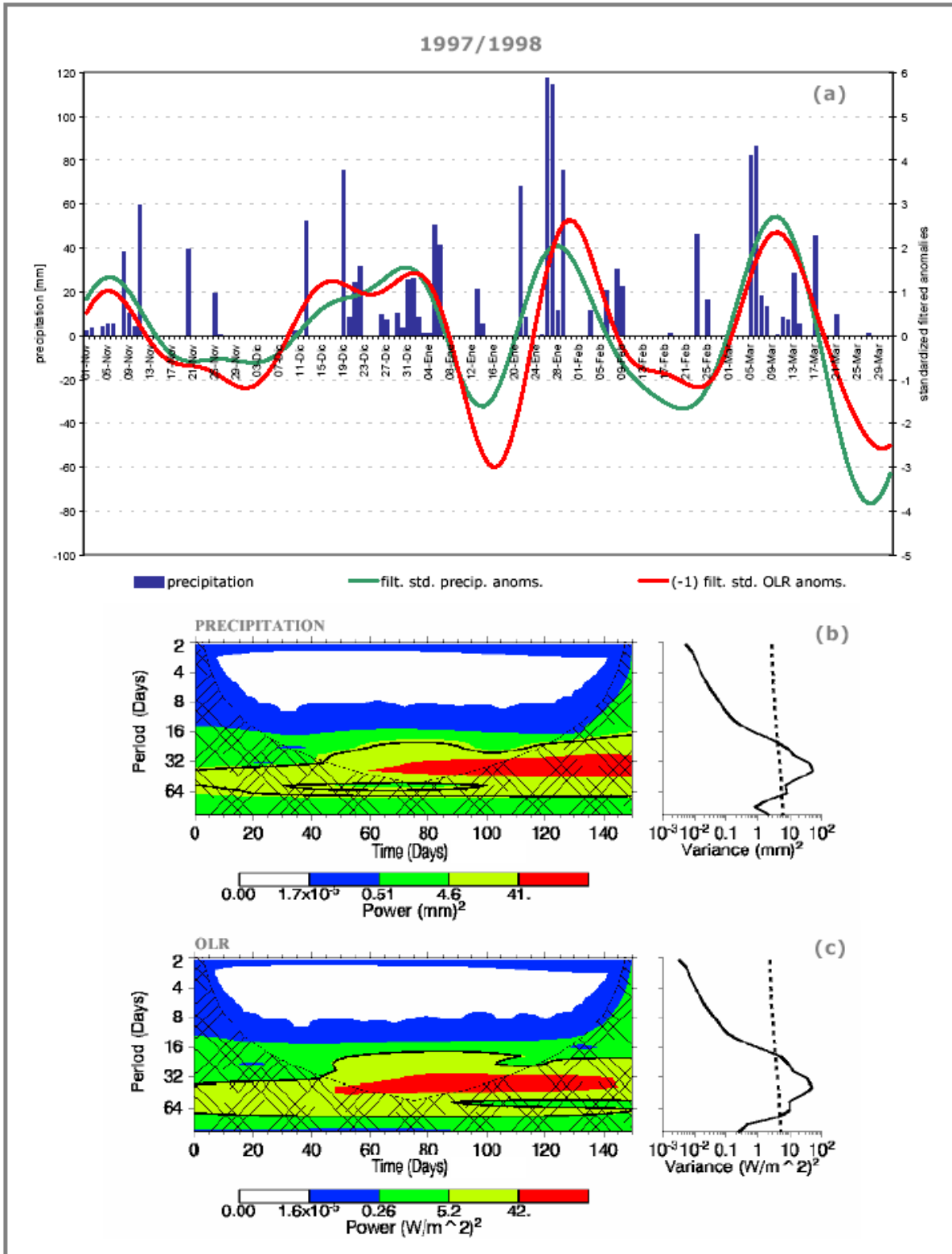


**Figure 3.** (a) Evolution of the timeseries during 1997-1998 summer season in Monte Caseros; (b) wavelet power spectrum and global wavelet for filtered precipitation; (c) wavelet power spectrum and global wavelet for filtered OLR. Black contour is the 5% significance level, using a white-noise background spectrum. The dashed line is the significance for the global wavelet spectrum, assuming the same significance level.

observed for all stations (not shown). OLR, however, shows a slight tendency for short events. Positive precipitation events tend to be short, with a mean length of 9.7 days. On the other hand, negative events of precipitation tend to be long, with a mean length of 10 days.

A timetable of precipitation events is presented Table 5 for Monte Caseros. It shows that both positive and negative events tend to be concentrated in the second half of the summer. This feature was also present in Corrientes station (not shown), and was not evident in the remaining stations analyzed. Table 5 also shows that negative events (yellow bands) tend to be longer than positive ones (green bands).

White dots on each event indicate the days on which the intraseasonal signal reached a peak (maximum if positive and minimum if negative). Those dates were then used to construct the composite analysis discussed in the following section.

### 3.5 Composite analysis

In order to study the dynamical characteristics of intraseasonal variability, composites of filtered OLR (20-90 days band-pass Lanczos filter), 850-hPa heights and 200-hPa heights were performed. Each of the dotted dates in Table 5 was considered as DAY 0.

The significance of such composites was assessed through a t-test, with the t statistic calculated as:

$$t = \frac{\text{comp}(V)}{S_v} \sqrt{N-1}$$

where  $\text{comp}(V)$  represents the variable composite value at each grid point,  $S_v$  the standard deviation in the same place and  $N$  the number of events considered.

Composites were constructed independently for short positive events (Figures 4a, 4b, 4c and 4d), long positive events (Figures 5a, 5b, 5c and 5d), short negative events (Figures 6a, 6b, 6c and 6d) and long negative events (Figures 7a, 7b, 7c and 7d).

#### a. Short positive events

Monte Caseros station registered 25 positive events of less than 10 days. Filtered OLR composites for those events show intense convection over northern Australia on 10 to 12 days before DAY 0. From around DAY -4, a configuration of inhibited SACZ and negative OLR anomalies over the region under study is observed, clearly resembling one of the SASS phases.

Geopotential-height anomaly composites show the activity of waves along the Pacific. These waves have an equivalent barotropic structure, as it can be seen by comparing the two levels. Around DAY -4 a cyclonic anomaly is seen to cross the Andes and establish over Argentina for several days. This perturbation is probably responsible for the positive precipitation event.

To understand the propagation features of these waves, a Hovmöller diagram was constructed; averaging in the band 40°S-60°S (Fig. 4d). Anomaly centers move rapidly to the east, and so does energy. It also shows, however, negative height anomalies near 60° W with quasi-stationary features.

#### b. Long positive events

Monte Caseros station registered 23 positive intraseasonal events of at least 10 days. Filtered OLR composites for these events show a similar situation than that observed for short events. What makes the difference is that in this case, the inhibited SACZ configuration appears to be preceded by an active SACZ phase, at around 10 to 15 days before DAY 0. Enhanced convection in the region under study becomes clear around DAY -4.

Geopotential-height anomaly composites also show a similar situation than for short events, but with stronger anomalies and a clearly defined wave train.

Propagation characteristics, as seen in Figure 5d are analogous than that observed for short events, but with stronger amplitudes.

#### c. Short negative events

24 negative events with lengths up to 9 days were observed in Monte Caseros station. Filtered OLR composites for those events are presented in Figure 6a. During the first days of the evolution, positive OLR anomalies are observed near the climatological location of the South Pacific Convergence Zone (SPCZ) and above the region under study. An active SACZ is observed through the evolution, but with quite a short activity period.

Composites for geopotential-height anomalies exhibit poorly organized perturbations. The Hovmöller diagram (Fig. 6d) shows that the anomalous centers act as pulses, which activate and weaken in only a few days, promoting the eastward energy propagation.



### Monte Caseros – short positive precipitation events – filtered OLR

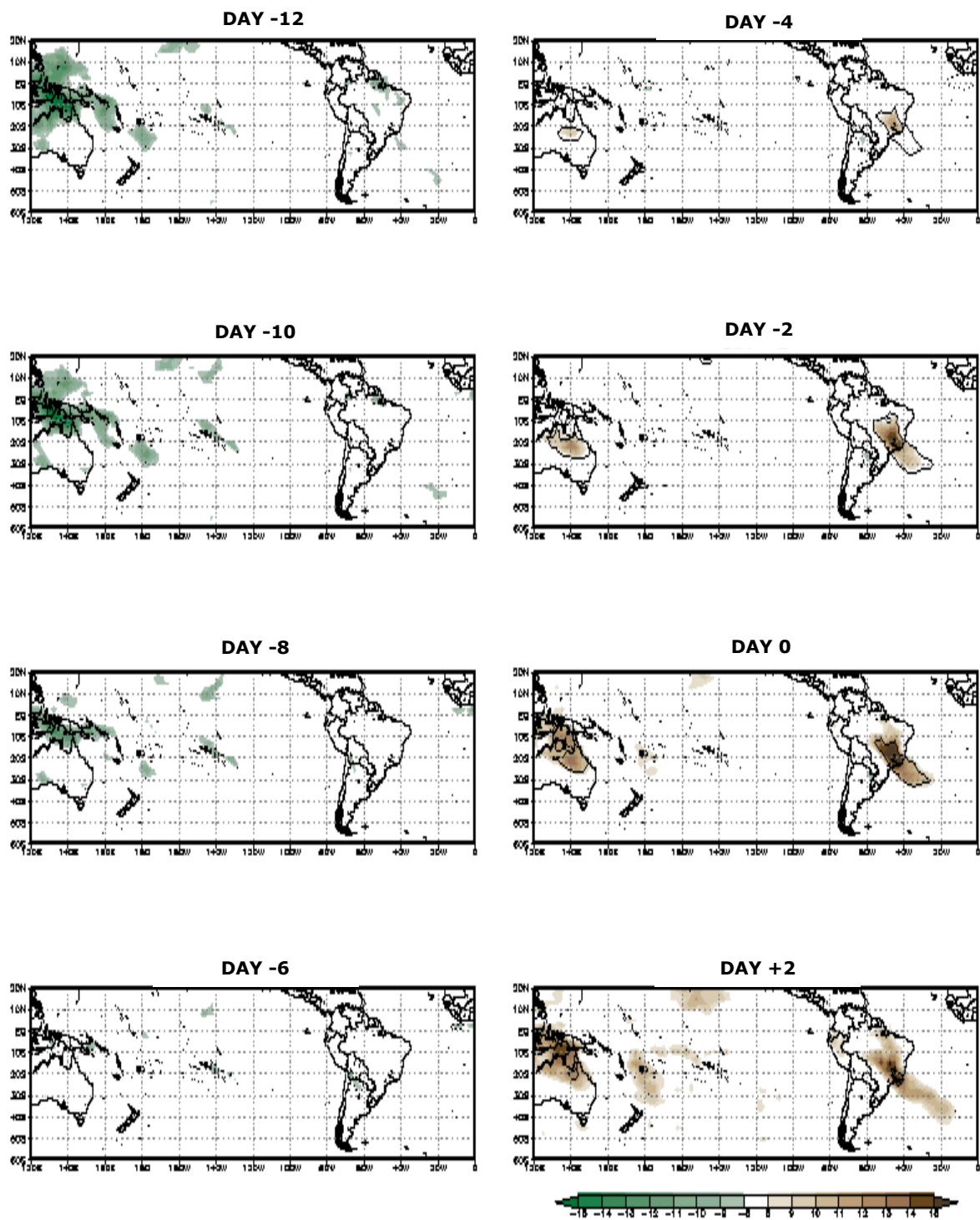


**Figure 4a.** Filtered OLR composites for short positive precipitation events in Monte Caseros station. Shading interval is  $1 \text{ Wm}^{-2}$  and small values are omitted. Black contour surrounds significant areas.

## Monte Caseros – short positive precipitation events – 850-hPa heights

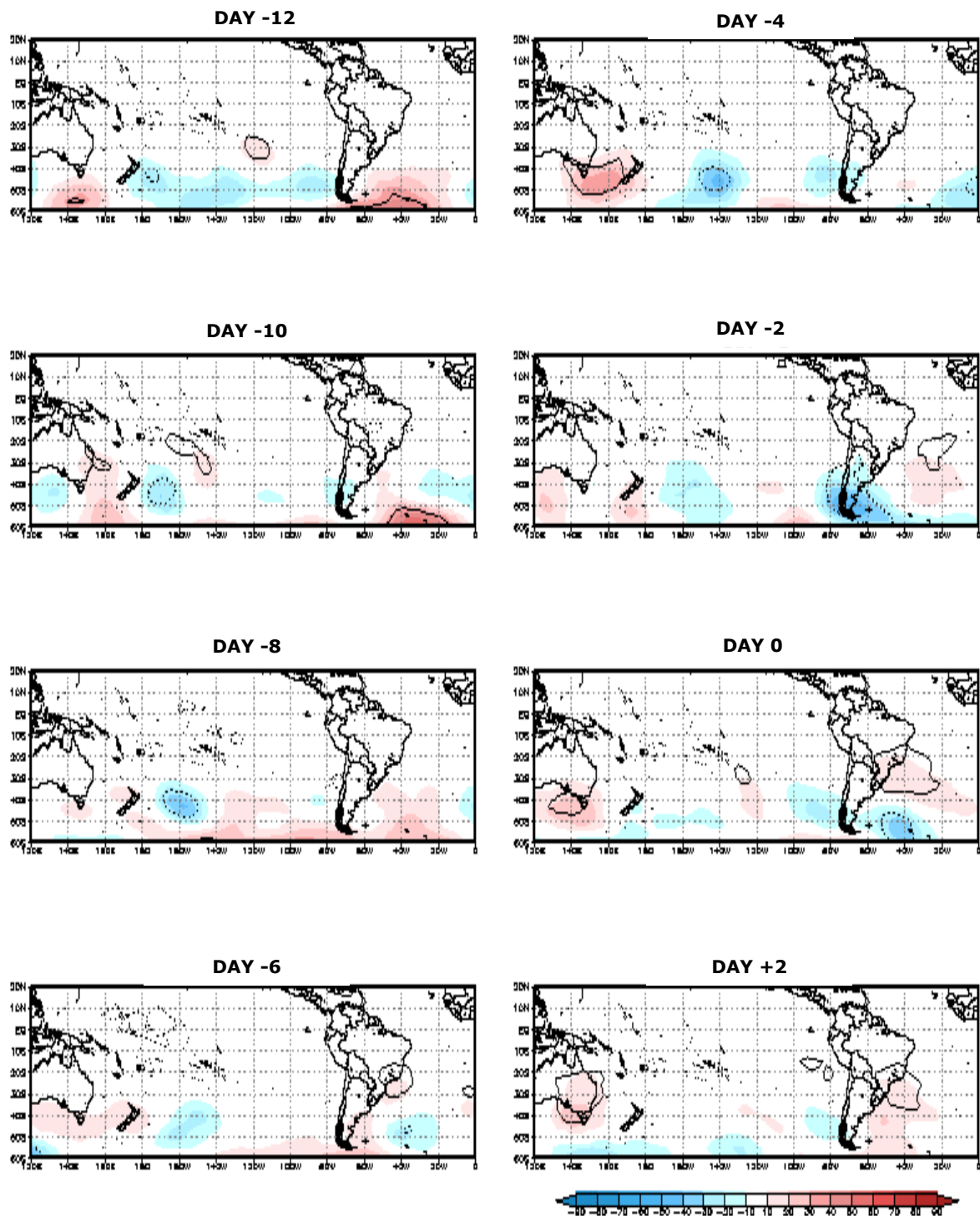


**Figure 4b.** 850-hPa heights composites for short positive precipitation events in Monte Caseros station. Shading interval is 10 m and small values are omitted. Black contour surrounds significant areas.

### Monte Caseros – short positive precipitation events – 200-hPa heights

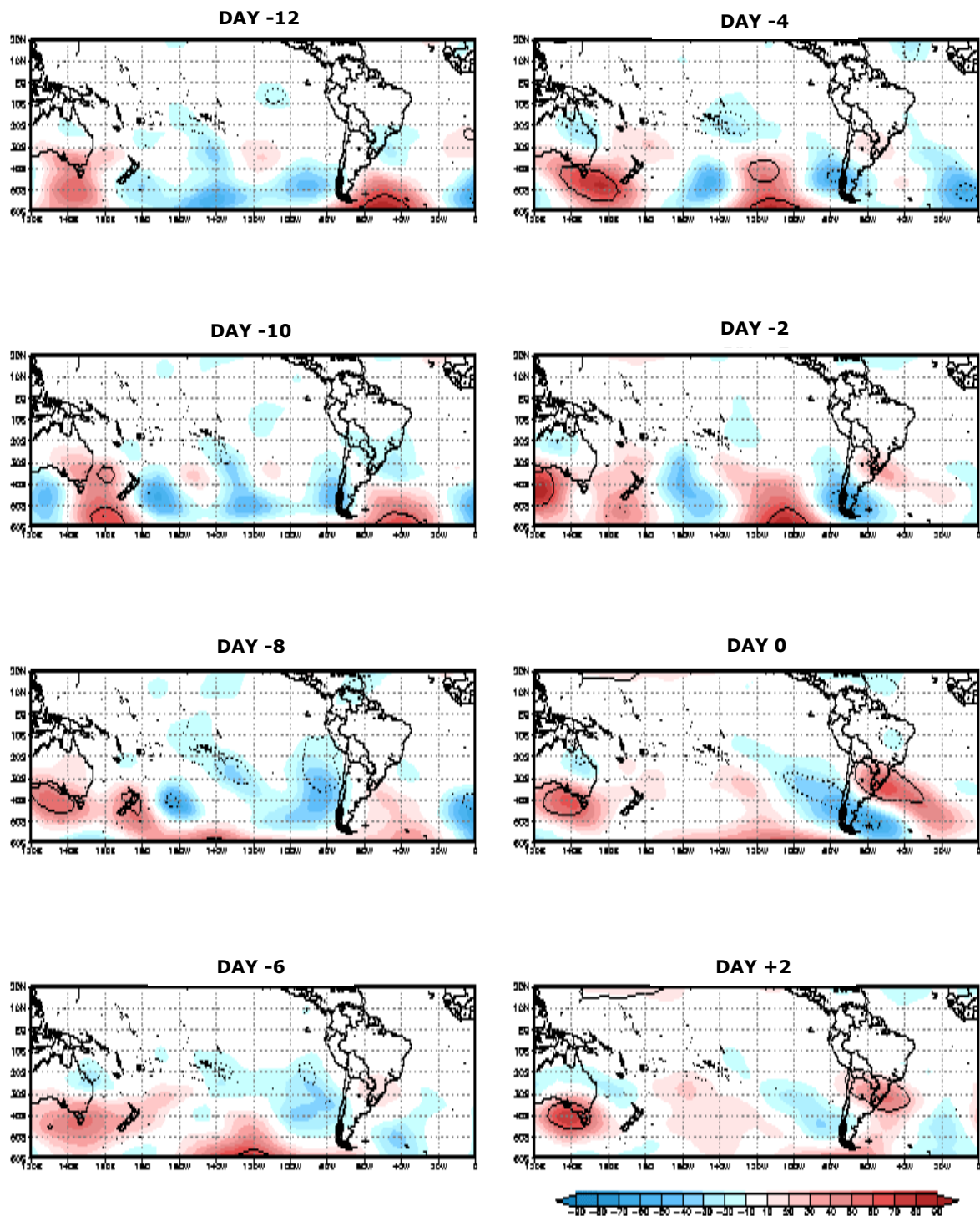
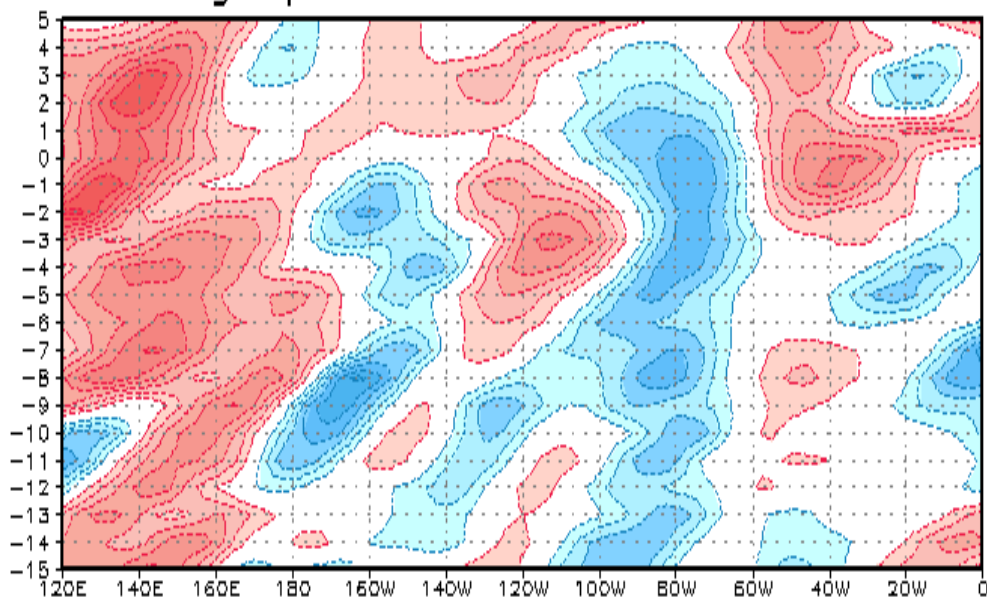


**Figure 4c.** 200-hPa heights composites for short positive precipitation events in Monte Caseros station. Shading interval is 10 m and small values are omitted. Black contour surrounds significant areas.

**Monte Caseros – short positive precipitation events**

geop. 200 hPa – 40S–60S



geop. 850 hPa – 40S–60S

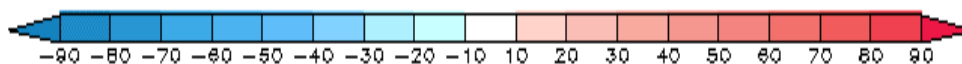
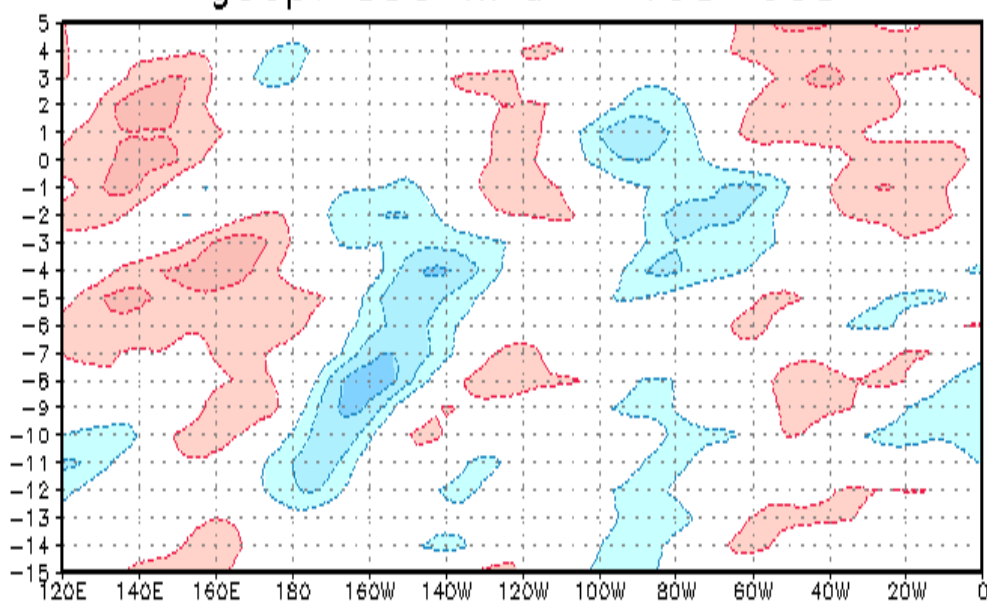


**Figure 4d.** Hovmöller diagrams for short positive precipitation events in Monte Caseros station. The averaging was performed between 40°S and 60°S. Contour interval is 10 m and zero contour was omitted.

### Monte Caseros – long positive precipitation events – filtered OLR

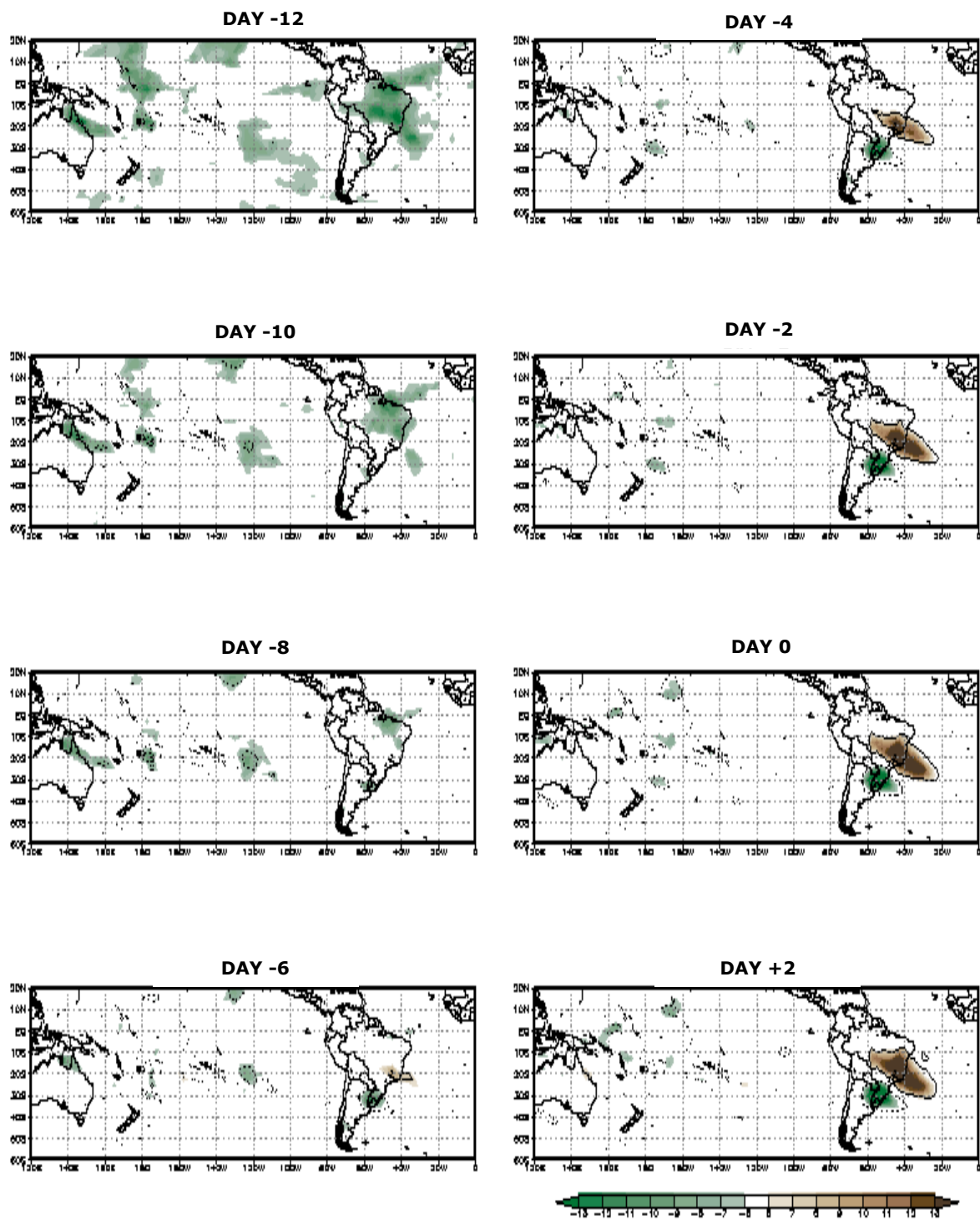


**Figure 5a.** Filtered OLR composites for long positive precipitation events in Monte Caseros station. Shading interval is  $1 \text{ Wm}^{-2}$  and small values are omitted. Black contour surrounds significant areas.

### Monte Caseros – long positive precipitation events – 850-hPa heights

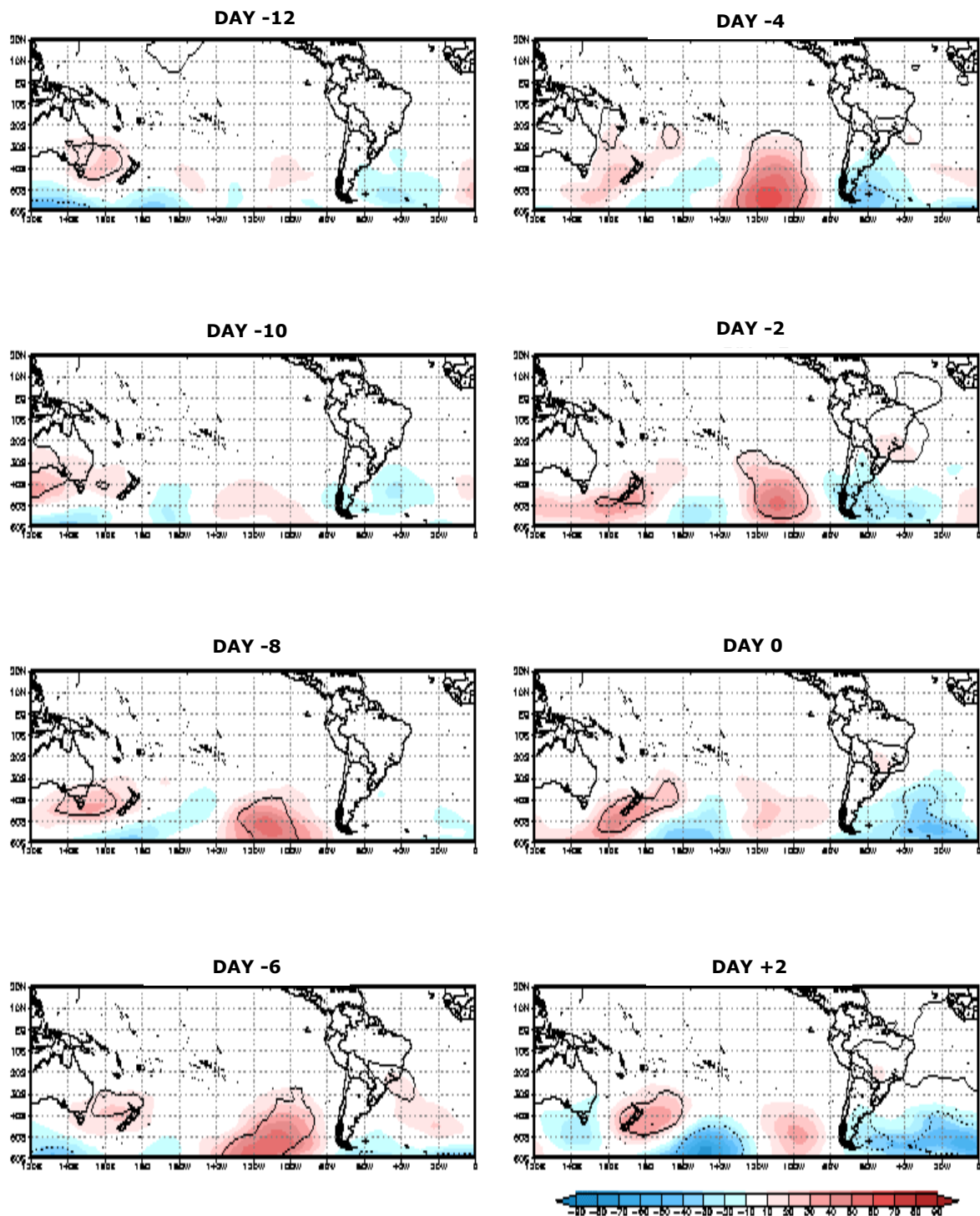


**Figure 5b.** 850-hPa heights composites for long negative precipitation events in Monte Caseros station. Shading interval is 10 m and small values are omitted. Black contour surrounds significant areas.

### Monte Caseros – long positive precipitation events – 200-hPa heights

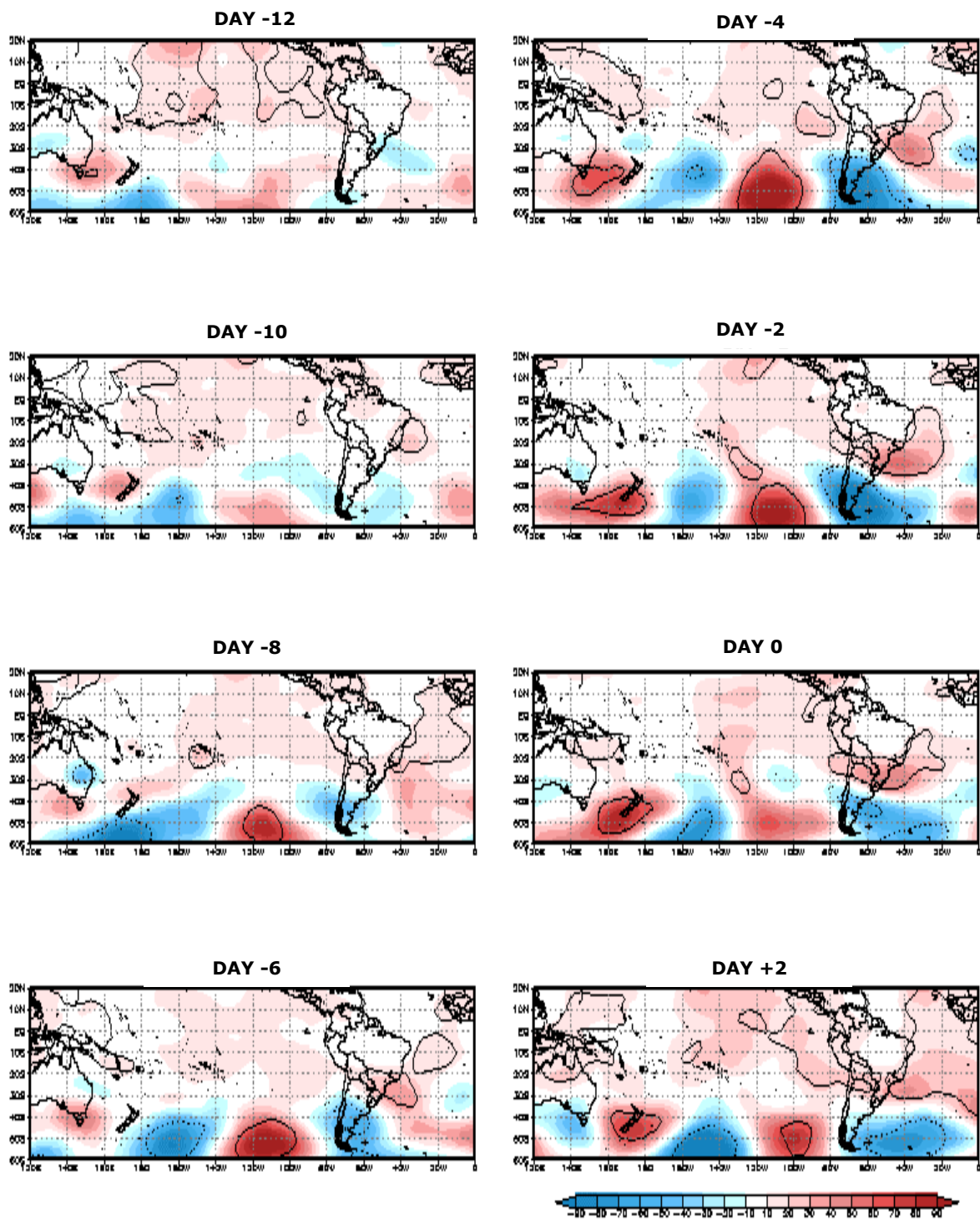
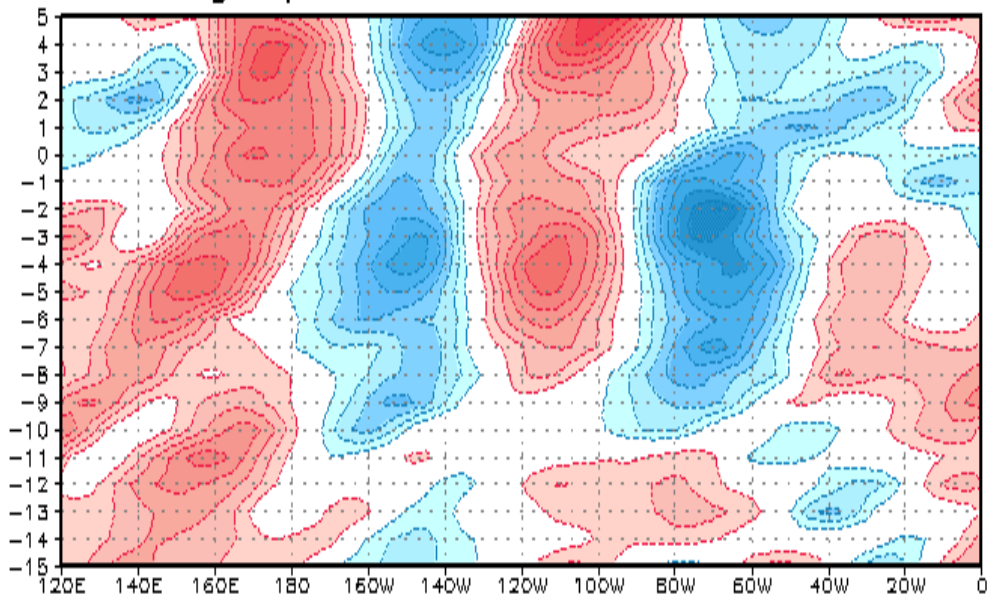


**Figure 5c.** 200-hPa heights composites for long positive precipitation events in Monte Caseros station. Shading interval is 10 m and small values are omitted. Black contour surrounds significant areas.

Monte Caseros – long positive precipitation events

geop. 200 hPa – 40S–60S



geop. 850 hPa – 40S–60S

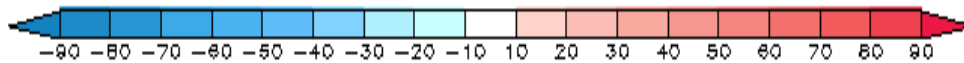
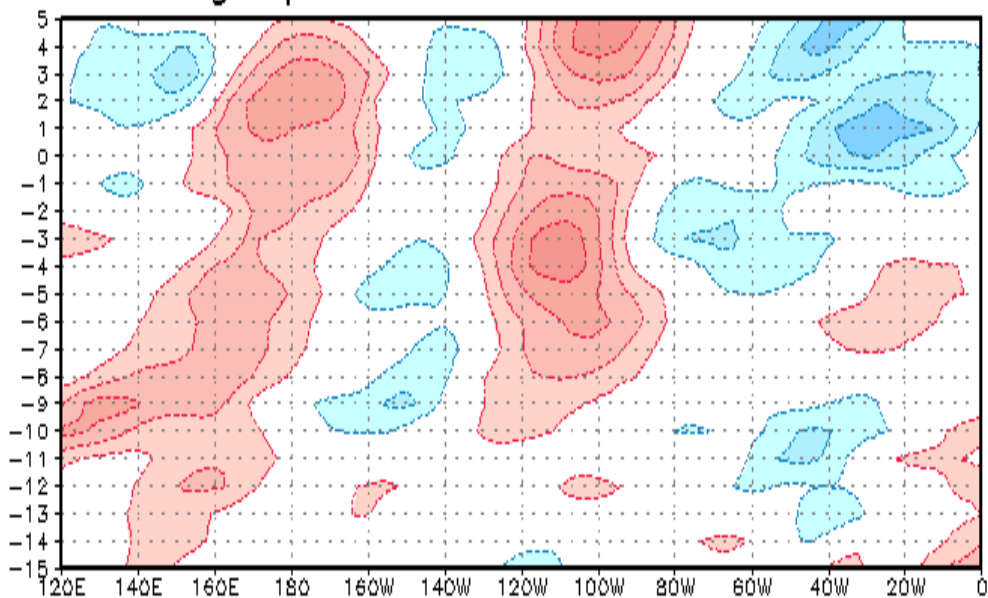


**Figure 5d.** Hovmöller diagrams for long positive precipitation events in Monte Caseros station. The averaging was performed between 40°S and 60°S. Contour interval is 10 m and zero contour was omitted.

### Monte Caseros – short negative precipitation events – filtered OLR

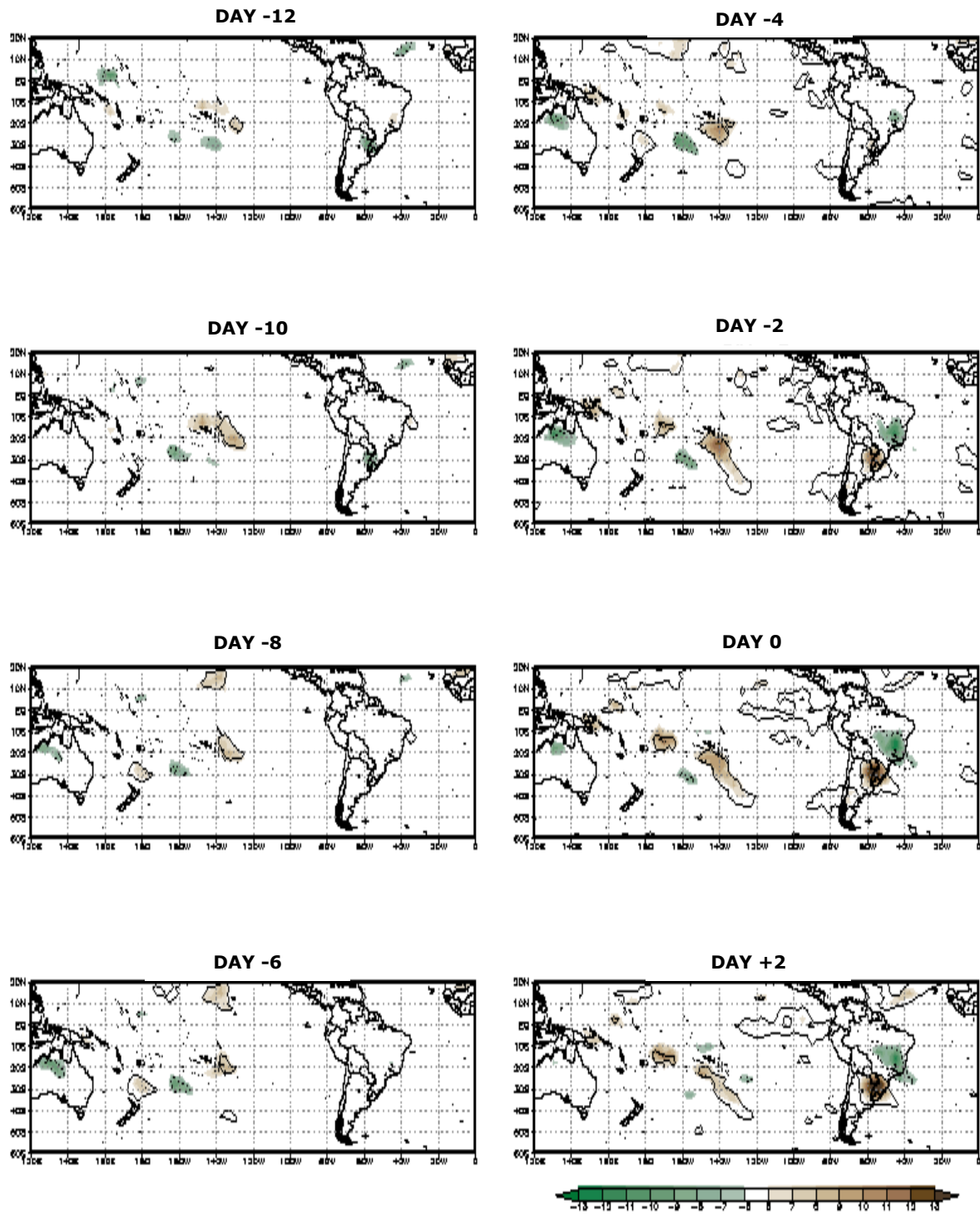


**Figure 6a.** Filtered OLR composites for short negative precipitation events in Monte Caseros station. Shading interval is  $1 \text{ Wm}^{-2}$  and small values are omitted. Black contour surrounds significant areas.

### Monte Caseros – short negative precipitation events – 850-hPa heights

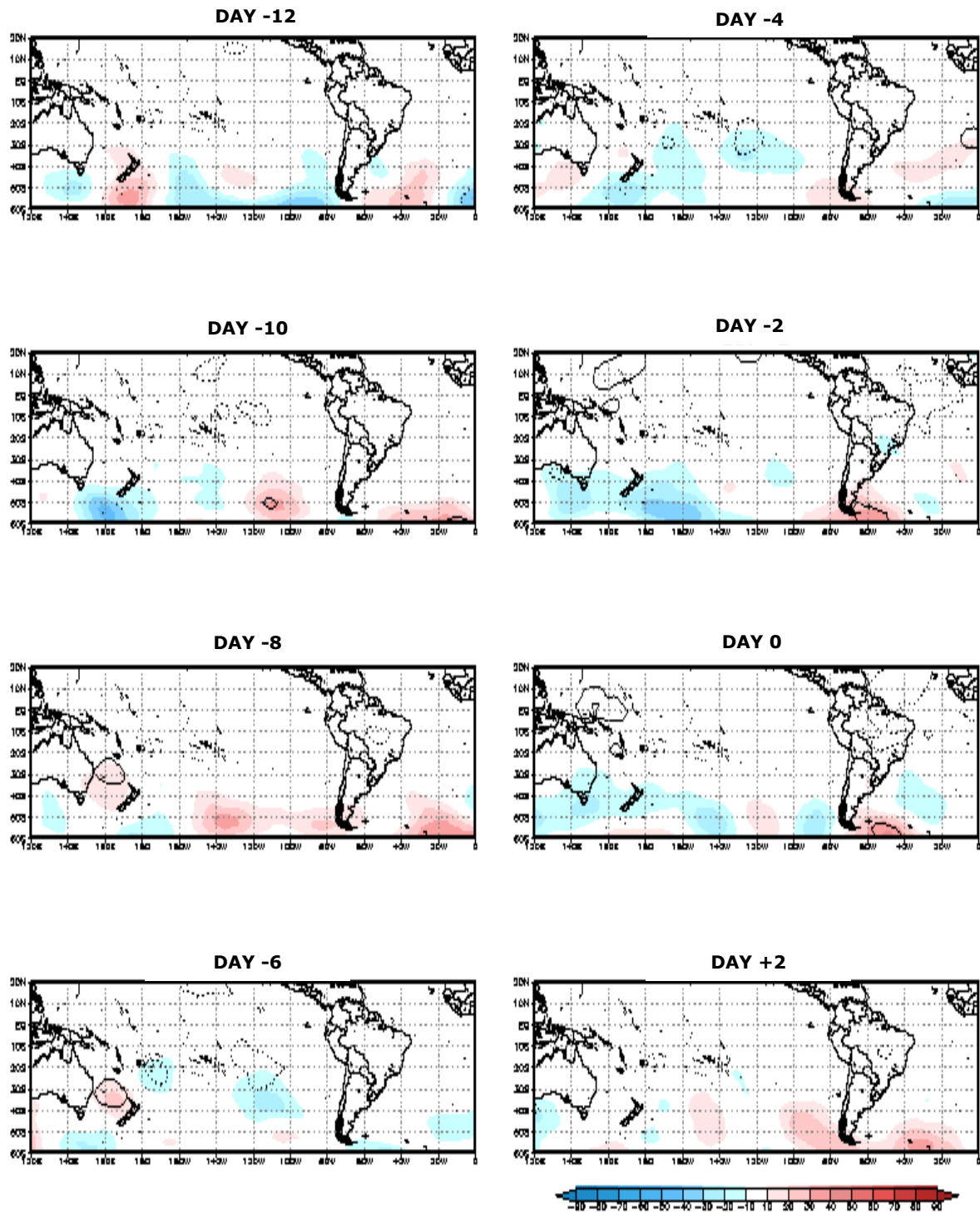


**Figure 6b.** 850-hPa heights composites for short negative precipitation events in Monte Caseros station. Shading interval is 10 m and small values are omitted. Black contour surrounds significant areas.

### Monte Caseros – short negative precipitation events – 200-hPa heights

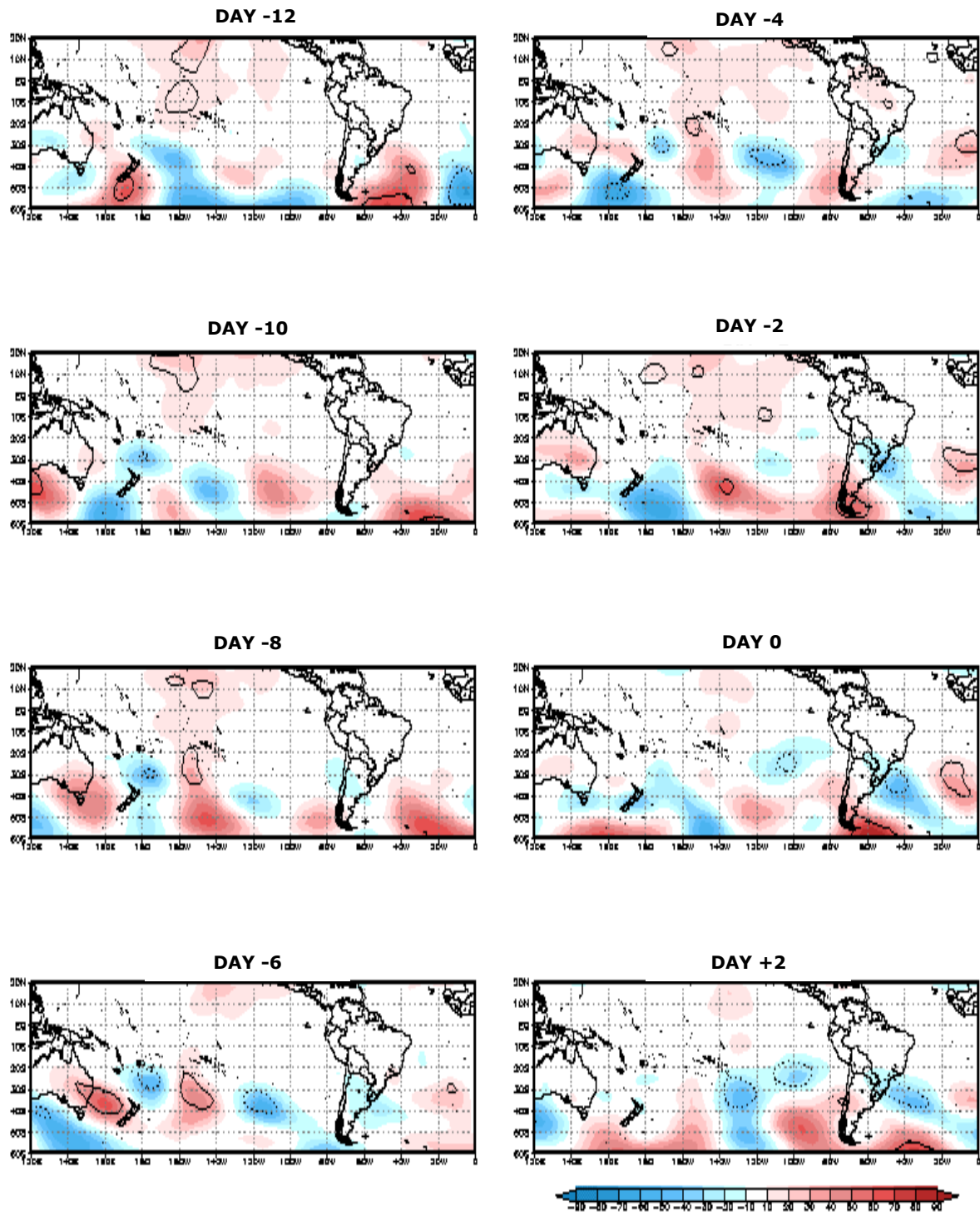
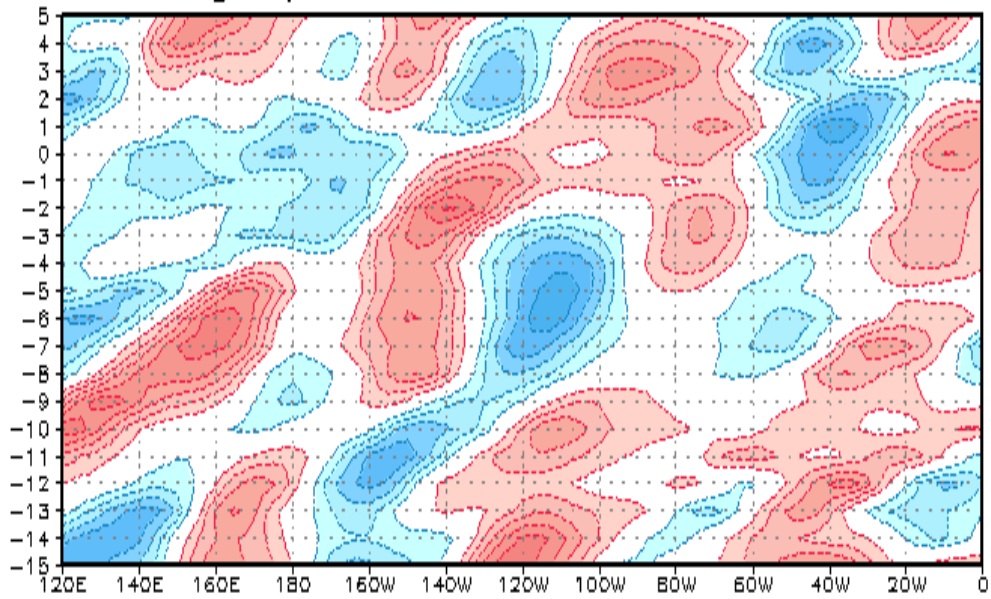


**Figure 6c.** 200-hPa heights composites for short negative precipitation events in Monte Caseros station. Shading interval is 10 m and small values are omitted. Black contour surrounds significant areas.

Monte Caseros – short negative precipitation events

geop. 200 hPa – 40S–60S



geop. 850 hPa – 40S–60S

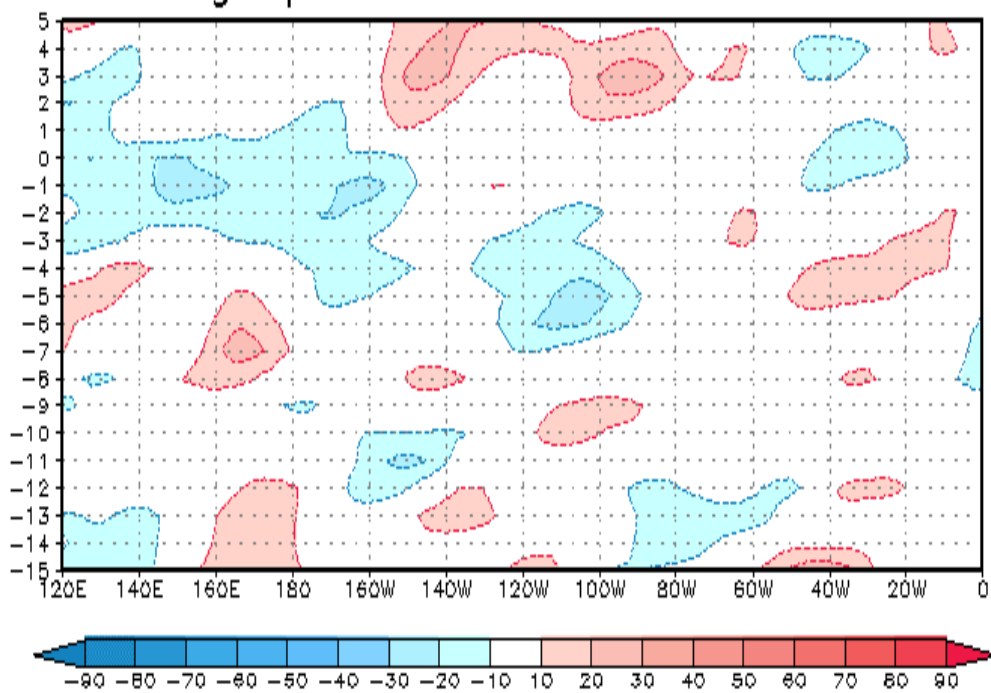


**Figure 6d.** Hovmöller diagrams for short negative precipitation events in Monte Caseros station. The averaging was performed between 40°S and 60°S. Contour interval is 10 m and zero contour was omitted.

### Monte Caseros – long negative precipitation events – filtered OLR

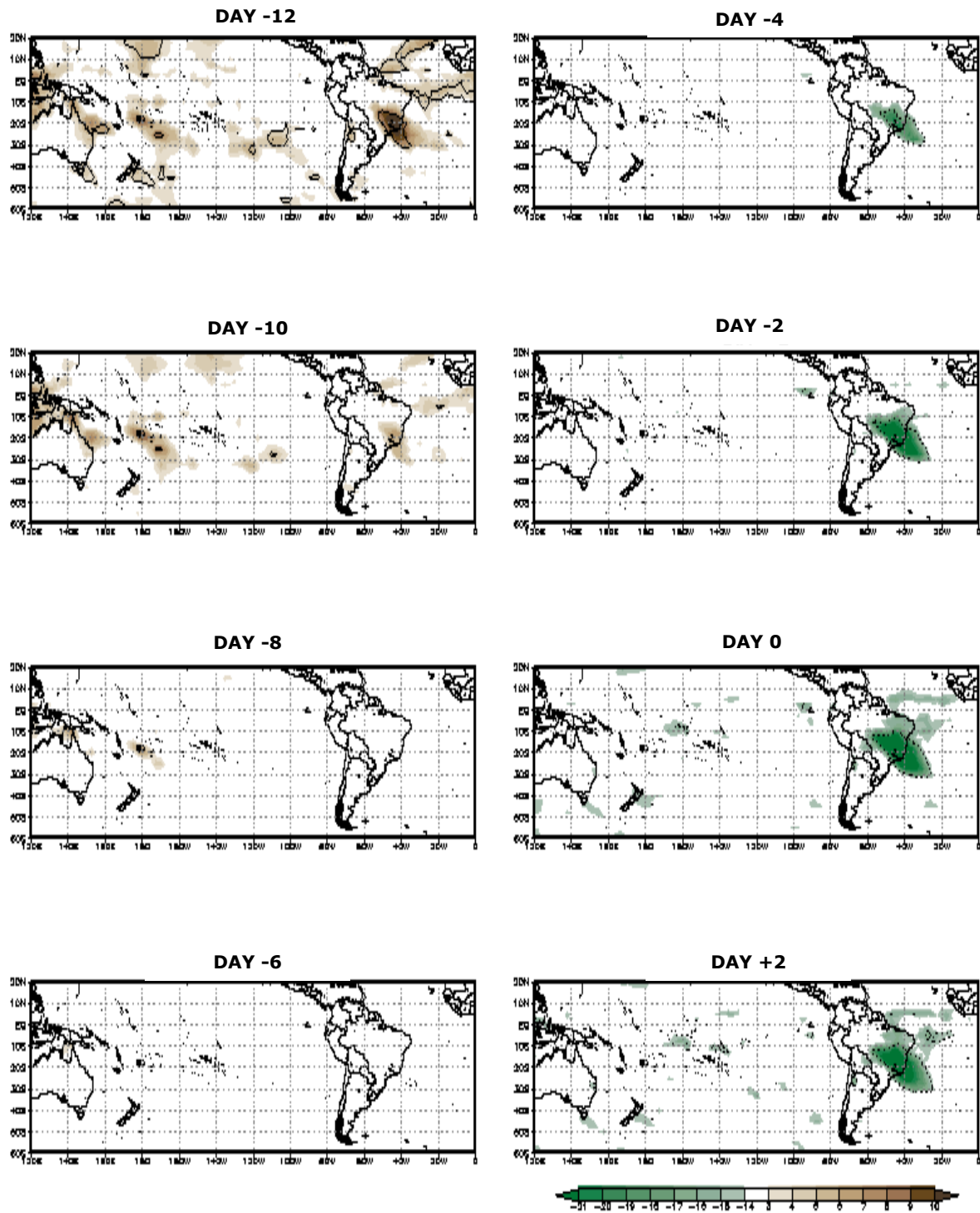


**Figure 7a.** Filtered OLR composites for long negative precipitation events in Monte Caseros station. Shading interval is  $1 \text{ Wm}^{-2}$  and small values are omitted. Black contour surrounds significant areas.

## Monte Caseros – long negative precipitation events – 850-hPa heights

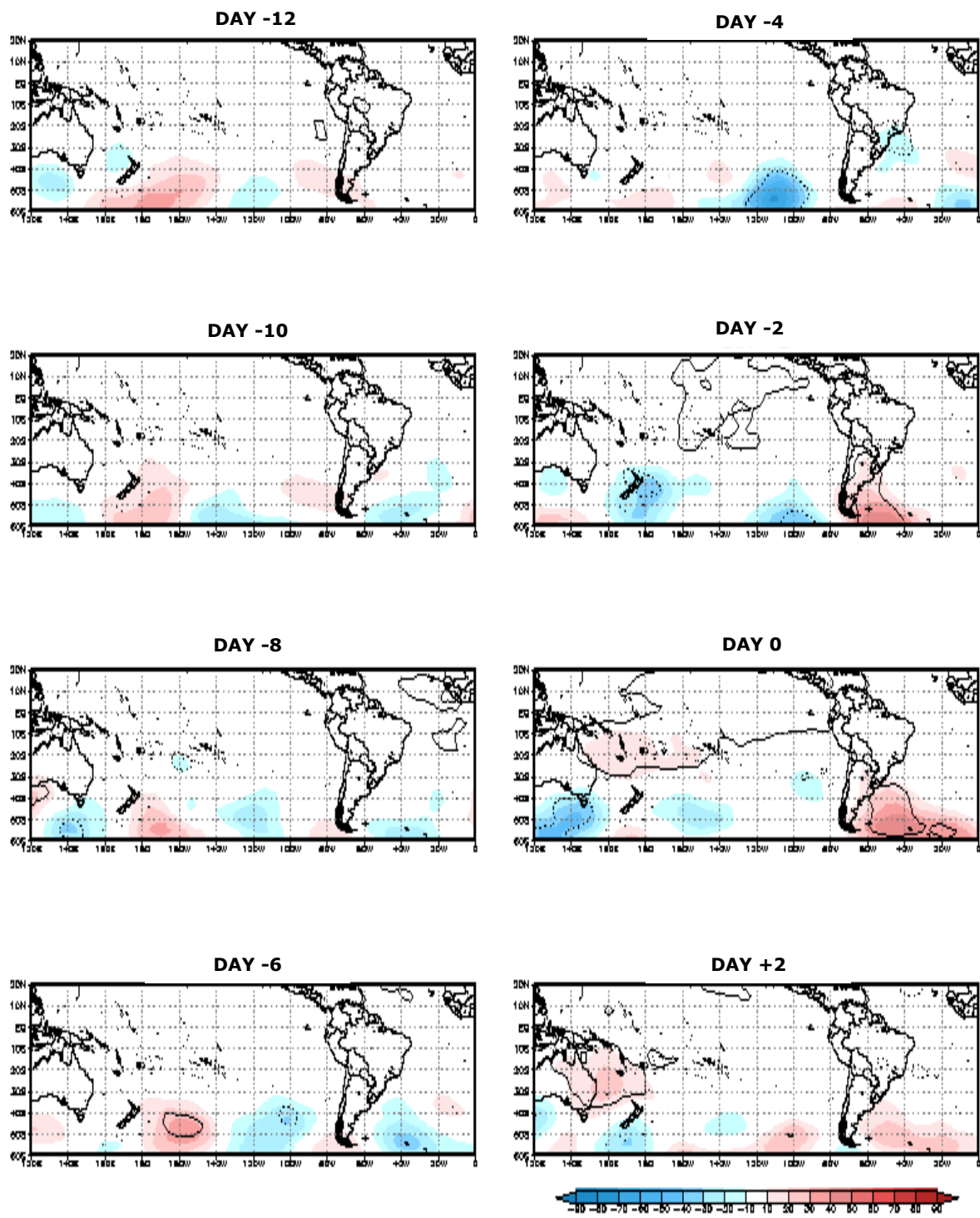


**Figure 7b.** 850-hPa heights composites for long negative precipitation events in Monte Caseros station. Shading interval is 10 m and small values are omitted. Black contour surrounds significant areas.

### Monte Caseros – long negative precipitation events – 200-hPa heights

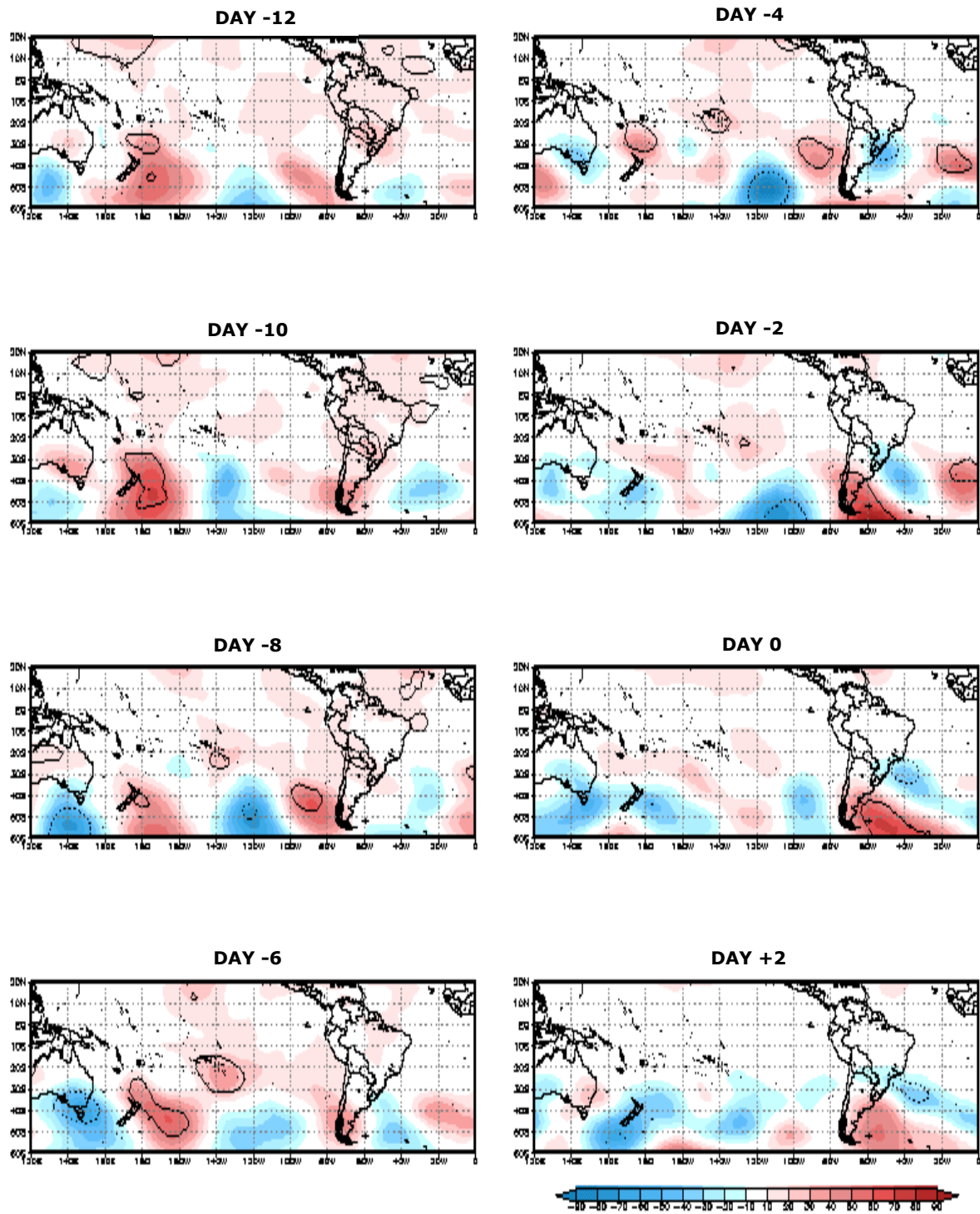


**Figure 7c.** 200-hPa heights composites for long negative precipitation events in Monte Caseros station. Shading interval is 10 m and small values are omitted. Black contour surrounds significant areas.

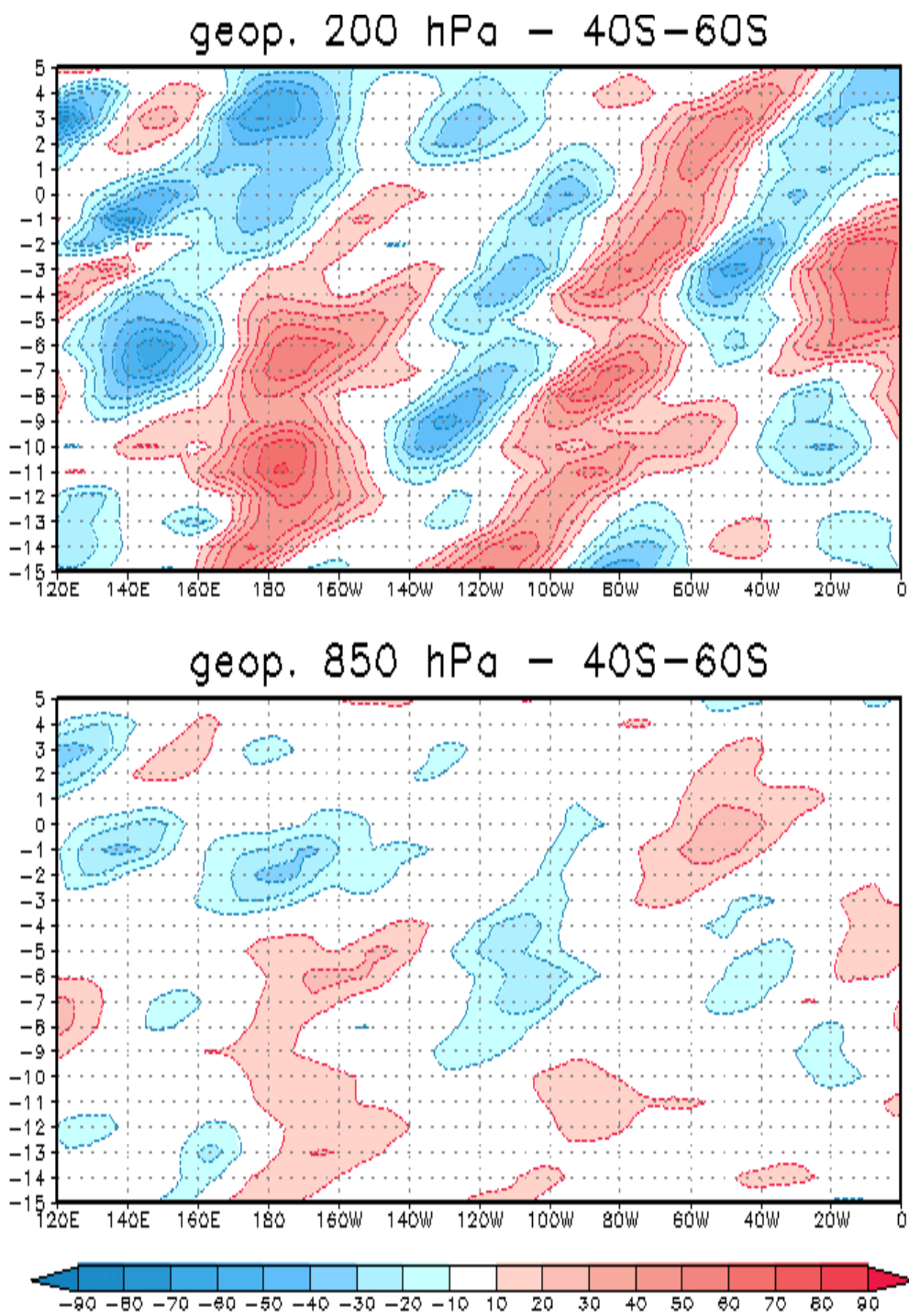


**Figure 7d.** Hovmöller diagrams for long negative precipitation events in Monte Caseros station. The averaging was performed between 40°S and 60°S. Contour interval is 10 m and zero contour was omitted.

#### d. Long negative events

Monte Caseros station registered 26 negative precipitation events of at least 10 days. Filtered OLR composites for those events is presented in Figure 7a. The situation evolves from positive anomalies north of Australia, in the SPCZ and the SACZ during the first days of the evolution, to a configuration with a particularly intense SACZ. It is important to remark that scale colors are not the same throughout this paper, and that explains the fact that in this case no positive anomalies are observed in the region under study.

Composites for geopotential-height anomalies show similar patterns to those observed for short events but with larger anomalies. Propagation features of these centers are also very similar, as can be seen comparing Figures 6d and 7d.

#### 4. CONCLUDING REMARKS

This work was meant to explore intraseasonal variability in daily precipitation timeseries from Argentinean National Weather Service stations. The results presented above led to the following conclusions:

- Intraseasonal variability explains a significant portion of summer precipitation variance in the selected stations.
- Wavelet analysis shows the existence of intraseasonal oscillations in precipitation timeseries, with periods ranging from 20 to 60 days.
- It was found that daily OLR variability explains a very small part of daily precipitation variability. For intraseasonal timescales, the study of particular summer seasons revealed that the agreement between OLR and precipitation fluctuations is important when the intraseasonal oscillations exhibit large amplitudes.
- Monte Caseros station responds to an intraseasonal variability regime with events concentrated in the second half of the summer. It also shows a tendency for positive events to be shorter than the negative ones. The mean frequency, however, is in both cases of around 2 events per summer.
- Composites of positive and negative precipitation events revealed that the first ones relate to the SASS pattern associated with an inhibited SACZ and enhanced convection in the subtropical plains. Negative events, however, are related to the opposite phase of the SASS pattern.

- Positive and negative precipitation events in Monte Caseros are linked to the activity of equivalent barotropic waves along the southern Pacific. In some cases, convection north to Australia seems to be forcing such wave activity.
- Short precipitation events in Monte Caseros seem to be preceded by convection to the north of Australia. Long positive events, however, follow a period of enhanced SACZ. Additionally, short positive events propagate faster than long ones.
- Some differences between short and long negative precipitation events in Monte Caseros were also found. While short events are preceded by inhibited convection north of Australia and in the SPCZ, short ones relate to a simultaneous weakening of both SPCZ and convection above the subtropical plains region.

#### ACKNOWLEDGEMENTS

This research was supported by UBA X264, NOAA-CLIVAR/PACS GC03-011, IAI-CRN55, ANPCyT/PICT-2004 No. 25269 and CONICET/PIP-5400.

#### REFERENCES

- Duchon, C. E., 1979: Lanczos Filtering in One and Two Dimensions. *J. Appl. Meteor.*, **18**, 1016-1022.
- Eshel, G., and B. F. Farrell, 2000: Mechanisms of eastern Mediterranean rainfall variability. *J. Atmos. Sci.*, **57**, 3219-3232.
- Ferranti, L., T. N. Palmer, F. Molteni, and E. Klinker, 1990: Tropical-extratropical interaction associated with the 30-60 day oscillation and its impact on medium and extended range prediction. *J. Atmos. Sci.*, **47**, 2177-2199.
- González, M. H. and V. R. Barros, 1996: Aspectos estadísticos del ciclo anual de precipitación y sus anomalías en Argentina subtropical. *Meteorológica*, **21**, Nro. 1 y 2, 15-26.
- Kalnay, E., and Coauthors, 1996: The NCEP/NCAR 40-Year Reanalysis Project. *Bull. Amer. Meteor. Soc.*, **77**, 437-471.
- Liebmann, B. and C. A. Smith, 1996: Description of a Complete (Interpolated) Outgoing Longwave Radiation Dataset. *Bull. Am. Meteor. Soc.*, **77**, 1275-1277.
- Liebmann, B.; G. N. Kiladis, J.A. Marengo, T. Ambrizzi and J.D. Glick, 1999: Submonthly convective variability over South America and the South Atlantic

- convergence zone. *J. of Climate*, **12**, 1877-1891.
- Liebmann, B.; G. N. Kiladis, C. Vera, A. C. Saulo, L. M. V. Carvalho, 2004: Subseasonal Variations of Rainfall in South America in the Vicinity of the Low-Level Jet East of the Andes and Comparison to Those in the South Atlantic Convergence Zone. *J. Climate*, **17**, No. 19, 3829-3842.
- Nogues-Paegle, J. and K.C. Mo, 1997: Alternating wet and dry conditions over South America during summer. *Mon. Wea. Rev.*, **125**, 279-291.
- Nogues-Paegle, J., L.A. Byerle, and K. C. Mo, 2000: Intraseasonal modulation of South American summer precipitation. *Mon. Wea. Rev.*, **128**, 837-850.
- Sardeshmukh, P. D., G. P. Compo and C. Penland, 2000: Changes of Probability Associated with El Niño. *J. Climate*, **13**, 4268-4286.
- Torrence, C. and G. P. Compo, 1998: A Practical Guide to Wavelet Analysis. *Bull. Amer. Meteor. Soc.*, **79**, 61-78.
- Trenberth, 1997: The Definition of El Niño. *Bull. Amer. Meteor. Soc.*, **78**, 2771-2777.